



1 **Implementation and application of an improved phase spectrum** 2 **determination scheme for Fourier Transform Spectrometry**

3 Frank Hase¹, Paolo Castracane⁵, Angelika Dehn⁵, Omaira Elena García⁷, David W. T. Griffith³, Lukas
4 Heizmann⁶, Nicholas B. Jones³, Tomi Karppinen⁴, Rigel Kivi⁴, Martine de Mazière², Justus Notholt⁶,
5 Mahesh Kumar Sha²

6

7 ¹IMKASF, Karlsruhe Institute of Technology (KIT), Eggenstein-Leopoldshafen, 76344, Germany

8 ²Royal Belgian Institute for Space Aeronomy (BIRA-IASB), Ringlaan 3, 1180 Brussels, Belgium

9 ³University of Wollongong, Wollongong, Australia

10 ⁴Space and Earth Observation Centre, Finnish Meteorological Institute, Sodankylä, Finland

11 ⁵European Space Agency, ESA/ESRIN, Frascati RM, Italy

12 ⁶Institute of Environmental Physics, University of Bremen, Bremen, Germany

13 ⁷Izaña Atmospheric Research Centre (IARC), State Meteorological Agency of Spain (AEMet), Santa Cruz de Tenerife,
14 Spain

15 *Correspondence to:* Frank Hase (frank.hase@kit.edu)

16 **Abstract.** Correct determination of the phase spectrum is a highly relevant task in Fourier Transform Spectrometry for
17 concluding which spectral distribution connects with the measured interferogram. We present implementation of an
18 improved scheme for phase determination in the operational Collaborative Carbon Column Observing Network (COCCON)
19 processor. We introduce a robust unwrapping scheme for retrieving a connected phase spectrum at intermediate spectral
20 resolution, which uses all spectral positions carrying enough signal to allow a significant determination of the phase. In the
21 second step, we perform a least squares fit of model parameters of a suited analytical phase spectrum model through all
22 reliable phase values constructed in the first step. The model fit exploits the fact that we expect the phase to be spectrally
23 smooth. Still, it can be refined to reflect specific characteristics inherent to the optical and electronic layout of the
24 interferometer. The proposed approach avoids the problems of the classical phase reconstruction method, which enforce a
25 spectrally smooth phase by directly limiting spectral resolution when calculating the complex phase. Thereby, the phase is
26 created from a very low number of interferogram points around the centerburst of the interferogram, which results in a
27 suboptimal noise propagation from the interferogram into the spectral domain. Moreover, the interpolation of the phase
28 spectrum across spectral subsections with reduced spectral signal is not well behaved and results depend strongly on the
29 numerical apodization function used for creating the low-resolution phase.



30 1 Introduction

31 Fourier Transform Spectrometry is an important technique for remote observation of atmospheric composition, especially in
32 the near and mid infrared spectral regions (then mostly referred to as Fourier Transform Infrared or shortly FTIR
33 spectroscopy). Ground-based networks contribute to the long-term monitoring of chemical composition, as the Network for
34 the Detection of Atmospheric Composition Change (NDACC) network [De Mazière et al., 2018], and the Total Carbon
35 Column Observing Network (TCCON) [Wunch et al., 2011] and the COllaborative Carbon Column Observing Network
36 (COCCON) [Frey et al., 2019; Sha et al., 2020; Alberti et al., 2022], which focus on the provision of precise and accurate
37 observations of column-averaged greenhouse and other climate and air quality relevant gas abundances. Moreover, highly
38 successful space borne sensors as Michelson Interferometer for Passive Atmospheric Sounding (MIPAS) onboard the
39 Environmental Satellite (ENVISAT) [Fischer et al., 2008], Atmospheric Chemistry Experiment – Fourier Transform
40 Spectrometer (ACE-FTS) onboard SCISAT [Bernath and al., 2005], and the Thermal And Near infrared Sensor for carbon
41 Observation – Fourier Transform Spectrometer (TANSO-FTS) onboard Greenhouse gases Observing SATellite (GOSAT)
42 [Yokota et al., 2009] and its successors have proven the usefulness of FTIR spectrometry for atmospheric observations.
43 Recently, the airborne imaging FTIR sensor Gimballed Limb Observer for Radiance Imaging of the Atmosphere (GLORIA)
44 for chemical and thermal limb imaging has been realized [Friedl-Vallon et al., 2014] and the imaging FTIR satellite mission
45 Changing Atmosphere Infrared Tomography (CAIRT) derived from GLORIA is under phase A study by ESA
46 [<https://www.cairt.eu>].

47 All FTIR spectrometers have in common that they use a two-beam interferometer for creating modulated intensity levels as a
48 function of the path difference between the two arms of the interferometer. The path difference is varied as function of time,
49 and during such a scan, the variable intensity is recorded by a detector element. By use of a co-recorded reference
50 modulation generated from a reference laser fed through the same interferometer, the variable intensity level recorded by the
51 infrared detector as function of time can be sampled as function of optical path difference x . It can be shown that the Fourier
52 Transform of the AC-coupled interferogram is associated with the spectral distribution of the incident radiation. If the
53 interferogram $I(x)$ would be symmetric around a common zero path difference (ZPD) of the interferometer for any
54 wavenumber ν , the spectral radiance as function of wavenumber $S(\nu)$ would be connected with the interferogram via a
55 simple cosine transform:

$$56 \quad 57 \quad S(\nu) \int_{x=-\infty}^{+\infty} I(x) \cos(2\pi\nu x) dx \quad (1)$$

58
59 We only claim a proportionality here for any selected wavenumber position, because from the practical viewpoint, the
60 determination of radiances in absolute units requires proper calibration measurements using reference sources providing a
61 known radiance level. This is a very laborious task and it is difficult to achieve sub-percent accuracy in the realization of
62 absolute units. In case of emission spectroscopy, this task needs to be solved, while atmospheric absorption spectroscopy



63 generally omits this procedure. In the case of absorption spectroscopy, the quantitative trace gas analysis is built on the local
64 contrast between absorption lines and adjacent continuum (assuming that the spectrometer offers sufficient spectral
65 resolution for resolving individual lines). Then, by assuming that the spectrally variable sensitivity of the spectrometer,
66 created by optical, detector, and electronic characteristics is spectrally smooth, no attempt is made for achieving ordinate
67 calibration. A section of the measured spectrum used for the trace gas analysis is then treated as a transmission spectrum, and
68 an empirical fit of continuum background is included in the analysis scheme. We do not further follow the problem of
69 ordinate calibration here, because it is not related to our aim of an improved phase reconstruction, which, however, can be
70 used for both absorption and emission spectroscopy.

71

72 In equation (1), we have extended the integration over all optical path differences. In practice, only a limited section up to a
73 maximum optical path difference (MPD) is accessible. The truncation of the interferogram is equivalent to a multiplication
74 with a boxcar function. This spectral response inherent to an FTIR spectrometer can be adjusted by applying a numerical
75 weighting function along the interferogram (the process of apodization). A proper description of the instrumental line shape
76 (ILS) is further complicated due to the presence of practical imperfections of the interferometer. Finally, we do not further
77 follow the problem of spectral ordinate calibration here, because it, too, is not closely related to our aim of an improved
78 phase reconstruction.

79

80 In order to provide a proper idea of the practical method of FTIR spectroscopy here, we further need to mention that the data
81 recording and processing is digital. An analogue-to-digital (ADC) converter is used to generate a digitized signal from the
82 detector signal. While sample-and-hold ADCs triggered by the laser sampling were used in the past, many manufacturers of
83 FTIR spectrometers today use widely available audio ADCs which offer high digitization depth (e.g. 24 bit) and add a final
84 interpolation step from the raw sampling equidistant in time domain into a sampling record equidistant in space [Brault,
85 1996]. In any case, the signal to be processed is discretely sampled, and in practice fast computational schemes for doing
86 discrete Fourier transforms are applied. Due to the discrete sampling process, integrals as shown in equation (1) become
87 sums and the bandwidth of the recorded signal needs to be properly limited in order to avoid aliasing.

88

89 A final aspect, which is closely connected to the considerations developed hereinafter, is the origin of the phase spectrum.
90 Due to residual optical asymmetry of the beamsplitter and possibly between the arms of the interferometer and due to
91 frequency dependent electronic delays, the resulting interferogram tends to be asymmetric and a global ZPD position
92 common to all wavenumbers does not exist. The electronic delays introduce both a shift between the laser reference and the
93 signal, as well as frequency-dependent delays in the infrared signal. This requires treatment of the Fourier Transform of the
94 real-valued interferogram as a complex quantity (so arising out of cosine and sine contributions) and thereby gives birth to
95 the concept of the phase spectrum. In complex notation, we can state

96



97 $s(\nu) = |s(\nu)|e^{i\varphi(\nu)} = \int_{x=-\infty}^{+\infty} I(x)e^{-i2\pi\nu x} dx$ (2)

98

99 The uncalibrated signal $s(\nu)$ now is a complex quantity. It can be separated into amplitude and phase $\varphi(\nu)$. The phase
100 spectrum $\varphi(\nu)$ describes how the phase angle of the harmonic oscillations which make up the interferogram evolves as
101 function of wavenumber. From the instrumental viewpoint, we expect the phase spectrum to be spectrally smooth, as the
102 impacting factors (optical dispersion and electronic delays) typically vary slowly as function of frequency.

103

104 The smoothness of the phase spectrum in near and mid-infrared FTIR spectroscopy is verified empirically on scales of
105 several to tens or even hundreds of wavenumbers (cm^{-1}). Given this, the simple approach of interpreting the absolute value of
106 the resulting complex spectrum as the measured spectral signal is clearly suboptimal in the presence of noise in the
107 interferogram. The assumption of uncorrelated white noise typically is adequate. This noise maps into white noise in the
108 complex spectrum. A contribution of $1/f$ noise might increase the noise amplitude towards low frequencies, and at very low
109 frequencies, source noise might become dominant. Therefore, working at higher scan speeds is generally preferred.

110

111 The assumption of a spectrally smooth phase allows to separate at each spectral position the complex spectrum into two
112 orthogonal components: the component along the direction we expect the spectral signal to be oriented, and the component
113 orthogonal to this direction. So, by exploiting the concept of a spectrally smooth phase, the noise mapped into the orthogonal
114 component can be avoided, only the noise along the signal component is unavoidable. Moreover, this approach avoids the
115 spectral noise floor of becoming a positive bias in opaque spectral subsections, as it would occur when simply using the
116 absolute value of the complex spectrum.

117

118 In order to make the scheme of a smooth phase a working concept, we not only rely on the assumption that it actually is
119 spectrally smooth, but we also need a practical approach for constructing a smooth phase spectrum with a noise level
120 significantly below the noise level of the complex spectrum. In practice, we achieve this by using only a short section of the
121 interferogram around ZPD. Thereby, the smooth phase spectrum is set by the equation

122

123 $|s(\nu)|e^{i\varphi(\nu)} = \int_{x=-\varepsilon \cdot MPD}^{+\varepsilon \cdot MPD} I(x)e^{-2\pi\nu x} \cdot A(x) dx$ (3)

124

125 Here, the dimensionless multiplier ε denotes that only a fraction of the complete interferogram recorded up to MPD is used.
126 The function $A(x)$ denotes a strong numerical apodization function, as any non-local ringing extending out from a spectral
127 position with high signal level would disturb the phase in the surrounding spectral region.

128



129 We finally need to mention that interferograms might be recorded “single-sided” or “double-sided”. Often, when an
130 interferometer is designed for achieving higher spectral resolution, the symmetry of the design is abandoned. Instead, the
131 ZPD position shifted near one end of the mechanical scan range, which still needs to be wide enough to reconstruct the phase
132 spectrum via equation (2), but the high-resolution details are inferred from the single remaining side of the interferogram
133 which is recorded. Our proposed method can be used in either situation, but it should be noted that in case of single-sided
134 interferogram recording, the error propagation of a residual phase error is much more critical, as sine contributions do not
135 cancel out (as one side of the interferogram is missing) [Braut, 1996; Brasunas and Cushman, 1997], so a very accurate
136 reconstruction is even more relevant in this case.

137

138 The reader finds detailed presentations of all the aspects of FTIR spectroscopy shortly summarized above in text books and
139 articles [Herres and Gronholz, 1985; Davis et al., 2001; Griffiths et al., 2007].

140

141 In section 2, we present the types of spectrometers we used to test the proposed phase correction method. Section 3 describes
142 a robust scheme for phase unwrapping and the fitting procedure for retrieving the parameters of the phase model. Section 4
143 investigates the characteristics of phase spectra for the spectrometers introduced in section 2.

144 **2 Materials and Methods**

145 This work has been performed in the framework of the FRM4GHG project (Fiducial Reference Measurements for
146 Greenhouse Gases; <https://frm4ghg.aeronomie.be/>) supported by European Space Agency (ESA) [Sha et al., 2020]. In the
147 framework of this project, among further topics related to fiducial reference measurements (FRM), the adequacy of different
148 portable spectrometers is investigated. Interferograms recorded with these spectrometers have been used for testing the
149 proposed phase reconstruction algorithm. We shortly present these spectrometers in the following.

150

151 The EM27/SUN Fourier-transform spectrometer (FTS) prototype has been developed by Karlsruhe Institute of Technology
152 (KIT) in cooperation with Bruker Optics, a well-known manufacturer of FTIR spectrometers. It uses a folded pendulum-
153 corner cube interferometer (“RockSolid” ® design) and employs two room temperature InGaAs detectors to cover the near-
154 infrared range from 4000 – 12 000 cm⁻¹. A solar tracker using Camtracker active feedback to control the position of the solar
155 image on the fieldstop of the spectrometer is directly attached to the spectrometer [Gisi et al., 2011]. Further instrumental
156 details of the EM27/SUN FTS design characteristics are provided by Gisi et al. (2012) and Hase et al. (2016). Since 2014,
157 the EM27/SUN FTS is available from Bruker as a commercial item. Meanwhile, more than hundred units are sold and are
158 operated worldwide by various working groups for atmospheric greenhouse gas measurements; they are especially suited for
159 the quantification of local sources as cities [Hase et al., 2015], coal mines [Luther et al., 2019; Luther et al., 2022], oil and
160 gas production areas [Kille et al., 2019], and landfills [Tu et al., 2022]. As an operational framework for guaranteeing



161 common instrumental and data analysis standards among the operators, the COCCON has been established since [Frey et al.,
162 2019; Alberti et al., 2022], which is significantly supported by ESA through FRM4GHG and further contracts.

163

164 The Bruker IRCube or “Matrix” FTIR is a compact OEM instrument operating in the mid or near IR regions and configurable
165 for a wide range of laboratory and industrial applications using a range of sampling accessories. In its basic form it contains
166 a folded pendulum-corner cube interferometer similar to the EM27/SUN (“RockSolid”[®] design) with 25mm beam diameter
167 and either 1 cm⁻¹ double-sided or 0.5 cm⁻¹ single-sided resolution. As used at the University of Wollongong for solar
168 measurements, the IRCube includes a source module which accepts a focussed input beam into a selectable aperture (the field
169 stop) and collimates it, the interferometer, and detector optics module focussing the parallel beam exiting the interferometer
170 onto a 1mm InGaAs detector via a short focal length off axis paraboloidal mirror. The solar beam is collected from a solar-
171 tracker-mounted telescope via a 20 m optical fibre – the beam exiting the fibre is focussed into the field stop of the IRCube’s
172 source module.

173

174 The Vertex70 spectrometer is produced and sold commercially by Bruker Optics. It was recently replaced in Bruker’s
175 production line by a successor named Invenio. One Vertex70 FTS was purchased in the framework of the FRM4GHG
176 campaign to be tested alongside the EM27/SUN and IRCube with the reference IFS125HR and AirCore measurements. The
177 Royal Belgian Institute of Space Aeronomy (BIRA-IASB) and the University of Bremen (UB) performed minor
178 modifications to the optical components of the Vertex70 and coupled it with a solar tracker to perform solar absorption
179 measurements. The feasibility to accommodate two detectors (InGaAs and InSb) in the spectrometer allows covering
180 simultaneously the near- and mid-infrared (NIR and MIR) spectral regions. The measured spectra are analysed to retrieve
181 column abundances of XCO₂, XCH₄, XCO and XH₂O in the NIR spectral region and column abundances of methane (CH₄),
182 nitrous oxide (N₂O), formaldehyde (HCHO) and carbonyl sulphide (OCS) in the MIR spectral region are currently studied
183 [Zhou et al., 2023; Sha et al., 2024]. The spectrometer showed comparable results for the retrieved trace gases as those
184 retrieved with the high spectral resolution FTIR spectrometers. An automated enclosure system has been developed to
185 deploy the spectrometers autonomously in the field and enhance the coverage of the fiducial reference FTIR data. The aim is
186 also to use it in future as a traveling standard improving consistency among FTIR data taken at different sites in the MIR
187 spectral region. The NIR retrieved target gases are part of the COCCON while the data retrieved in the MIR spectral range
188 can complement the NDACC-FTIR data. This activity is supported by ESA through FRM4GHG contracts.

189

190 The Izaña Observatory (IZO) is a high-mountain station located on the island of Tenerife (Canary Islands, Spain) in the
191 subtropical North Atlantic Ocean (28.3°N, 16.5°W) at an altitude of 2.37 km a.s.l. IZO is managed by the Izaña Atmospheric
192 Research Centre (IARC, <https://izana.aemet.es/>, last access: 5 August 2024), which belongs to the State Meteorological
193 Agency of Spain (AEMet). Within the IZO’s atmospheric research activities, the FTIR programme started in 1999 in the
194 framework of a collaboration between AEMET and KIT [Schneider et al., 2005], contributing to NDACC and TCCON



195 networks since 1999 and 2007, respectively. To do so, the IZO FTIR instrument, currently a Bruker IFS125HR based on a
196 Michelson interferometer, records high-resolution solar absorption spectra in the MIR region within NDACC activities and
197 in the NIR region for TCCON retrievals, using a set of different field stops, narrow-bandpass filters, and detectors
198 [Schneider et al., 2010; García et al., 2021].

199

200 For TCCON the IFS125HR FTIR measures between 4000 and 10,000 cm^{-1} at a spectral resolution of 0.02 cm^{-1} (MPD of 45
201 cm) using a calcium fluoride (CaF_2) beamsplitter, an extended Indium–Gallium–Arsenide (InGaAs) photodiode detector
202 operated at room temperature, and no optical filters. The operational TCCON spectra are the result of co-adding six single-
203 sided interferograms in order to increase the signal-to-noise ratio. These interferograms are acquired with a scanner velocity
204 of 20 kHz, so the acquisition of one solar spectrum lasts about 4 minutes.

205

206 **3 New Phase reconstruction scheme**

207 The drawback of the classical method described in the introduction is twofold. (1) The reduction of the phase spectrum to the
208 desired very low resolution is achieved explicitly by using a very short section of the interferogram around ZPD for the
209 Fourier transform [Mertz, 1965; Forman et al., 1966]. This approach neglects interferogram data points further out which
210 still could contribute information on the phase. (2) The resulting spectral interpolation as part of the procedure is not well-
211 defined especially across spectral sub-regions of increased opacity, as they occur in solar absorption spectroscopy between
212 the atmospheric window regions and in strong absorption bands. Because the phase spectrum across such a region is strongly
213 impacted by the overlapping contributions to the phase emerging from either side of the opaque region, the outcome for the
214 phase at a certain spectral position in the region with reduced transmission will depend on the user-selected resolution for the
215 phase calculation and the chosen apodization function.

216

217 We will achieve our enhanced reconstruction of the phase spectrum by fitting a smooth parameterized phase model through a
218 calculated phase spectrum, which preserves higher spectral resolution than required for the desired degree of spectral
219 smoothness. The smoothness of the phase spectrum is ensured by the phase model used, while avoiding the aforementioned
220 problems of the classical method. We use a least squares fit of the model to the raw phase spectrum, which is a well-defined
221 process with respect to interpolation. A similar method has been proposed by Learner et al., 1995, in the context of emission
222 spectra.

223

224 The phase spectrum is a function of angular orientation, so it is invariant under phase shifts of size $\pm 2\pi n$, with $n = 1, 2, 3, \dots$
225 For our fit procedure, we need to ensure that the raw phase used as input does not include jumps between such branches. We
226 suggest the very robust procedure summarized as procedural steps in Table 1.



227 This proposed method can fail if the phase difference calculated in step 5 is greater than $\pm\pi$. We did not encounter this
 228 situation, but it may occur if the phase slope is very steep and can possibly be avoided by appropriate repositioning of the
 229 ZPD point when calculating the Fourier Transform.

230

231 Table 1: step-by-step procedure for developing the raw phase used as input for the model fit.

Step #	Procedure	Comment
0	Allocation of arrays: (1) float array for accepting phase values (2) logical array indicating availability of valid phase value	
1	Establish the noise level and the size of potential artefacts superimposed on the spectral signal. Set a threshold T for the subsequent phase calculation significantly above noise and artefact levels.	
2	Search for position of max amplitude of $s(\nu_i)$ in the complex signal in the optical bandpass.	Restrict search to relevant optical bandpass, as out-of-band artefacts triggered by source brightness fluctuation might create very big amplitudes at $\nu \approx 0$.
3	Calculate phase at spectral index $istart$ with max signal amplitude.	Use a quadrant-sensitive $atan2$ function on real and imaginary part of the complex signal.
4	Move from current position one spectral index up. If still within the defined spectral bandwidth, check whether $s(\nu_i) > T$. If so, set logical array value of current position to <i>true</i> , otherwise to <i>false</i> .	
5	If the logical array value of the current position i is <i>true</i> , calculate the phase difference between the nearest preceding point j assigned <i>true</i> and the current position.	Use the value of the cross product between the normalized complex pointers: $\Delta\varphi(j \rightarrow i) = \text{asin} \left\{ \frac{(s(\nu_j) \times s(\nu_i))}{ s(\nu_j) s(\nu_i) } \right\}$
6	Calculate the new phase value at the current position using the phase value of the nearest preceding point	$\varphi(i) = \varphi(j) + \Delta\varphi(j \rightarrow i)$
7	Continue steps 4 + 5 + 6 until the upper limit of the spectral bandwidth is reached.	



8	Return to position <i>istart</i> and use the corresponding procedure in downwards direction until the lower limit of the spectral bandwidth is reached.	
---	---	--

232

233

234 The second step is to fit the parameters of the phase model to the raw phase values. We assume here use of a model linear in
235 the model parameters to be fitted. However, nonlinear models also can be handled in our approach by implementing an
236 iterative search for the optimal model parameter values. If a sophisticated model is chosen, which intends to describe actual
237 physical characteristics of the spectrometer (dispersion curves, electronic response characteristics) and retrieves physical
238 quantities (layer thicknesses, capacitances, resistor values), using a model which is nonlinear in the parameters might be
239 unavoidable. When constructing ad-hoc models which simply enforce smoothness, the choice of a simple linear model seems
240 advisable. The fitting procedure needs to be restricted to points for which valid phase values were established in the previous
241 step. The fitting procedure can take into account a weighting according to the squared signal amplitude. We found very little
242 effect of including this refinement in the determination of model parameters, so we did not implement it in the current pre-
243 processing scheme. Taking a weighting into account, the equation for fitting the phase model parameters becomes

244

$$245 \vec{p}_{model} = (K^T W K)^{-1} K^T W \vec{\varphi}_{raw} \quad (4)$$

246

247 Here, \vec{p}_{model} is the set of model parameters, K is the Jacobean matrix, which holds the derivatives of the phase model at each
248 spectral grid point with valid raw phase entry, W is a diagonal matrix with $\frac{1}{(s(v_i))^2}$ entries (again, for each spectral grid point
249 with valid raw phase entry), and $\vec{\varphi}_{raw}$ is the vector containing all valid raw phases. Note that the vector dimension of $\vec{\varphi}_{raw}$
250 and \vec{p}_{model} differ, as after receiving the set of model parameters, \vec{p}_{model} can be calculated at all spectral positions, including
251 interpolation across near opaque spectral sections and extrapolation beyond the first or last spectral point found in the optical
252 bandpass. The predicted model phase values further outside of the relevant spectral bandpass are meaningless and might be
253 suppressed altogether (by allocating the array for \vec{p}_{model} to fit the relevant spectral bandpass).

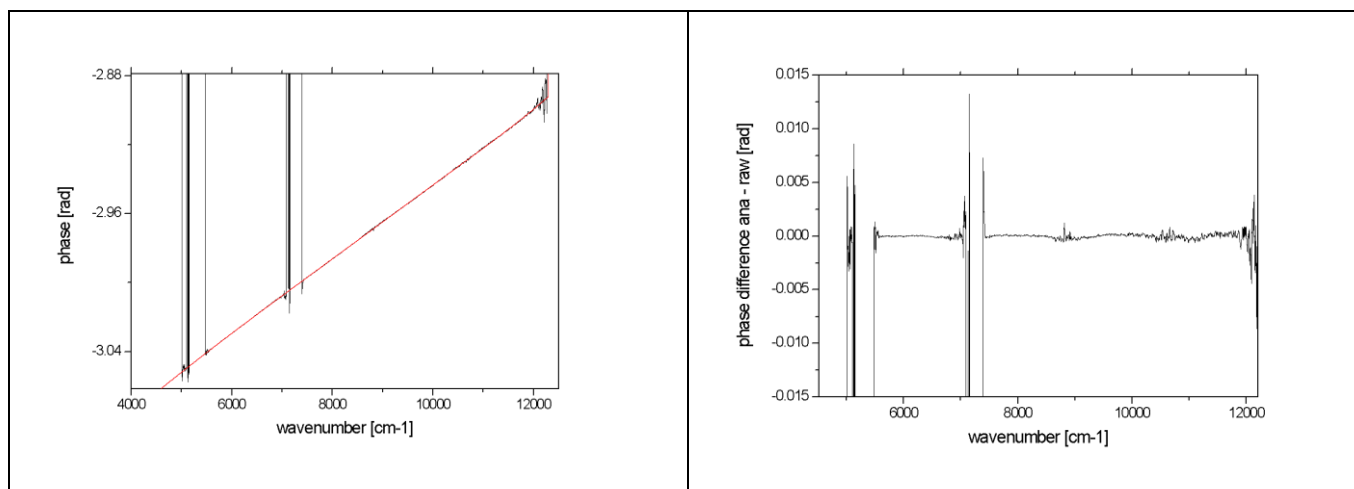
254 4 Results

255 For the actual work on the FTIR spectrometers introduced in section 2, we used a polynomial model of order 7. The raw
256 phase calculation uses a resolution of about 10 cm^{-1} , which is supported by all spectrometers we included in the study
257 (sufficient number of points on the short side of the interferogram).



258 4.1 Phase spectrum of the EM27/SUN FTS

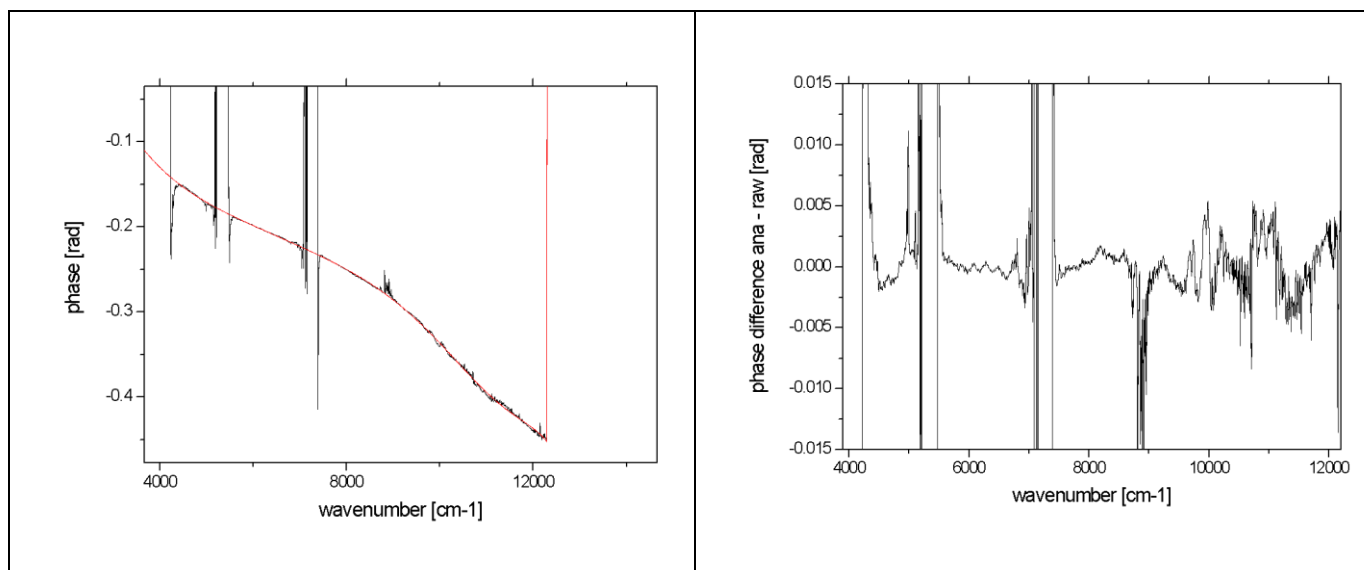
259 The results achieved for the EM27/SUN are shown in Figure 1. The spectrometer shows a remarkably linear phase spectrum
260 across the whole spectral region of the main detector (covering 5000 to 12000 cm^{-1}). The differences between the model fit
261 and the raw phase are below 1 mrad. The level of smoothness and linearity of the phase spectrum is outstanding among all
262 spectrometers tested. This behaviour probably is supported by the beamsplitter design. The same optical plate is passed twice
263 by the radiation, acting as substrate of the beam-splitting coating layer in one passage and as compensating plate in the other
264 passage. In addition to this, also the analogue electronic chain seems to introduce only minimal dispersion due to runtime
265 effects. It is not clear why the other spectrometers investigated here, all built by the same manufacturer, show significantly
266 stronger structures in the phase spectrum.



267
268 Figure 1: EM27/SUN phase spectrum. Left panel: raw phase (black) and fitted model (red). Right panel: difference between
269 model (analytical, ana) and raw phase (raw). The gaps in the raw phase are due to opaque spectral sections.

270 4.2 Phase spectrum of the IRCube FTS

271 The phase spectrum of the IRCube is shown in Figure 2. The spectral bandpass covers the range of 4000 to beyond 12 000
272 cm^{-1} . The differences between the phase model and the raw phase show more structure than in case of the EM27/SUN, but
273 still, these oscillatory features are largely within 2 mrad.



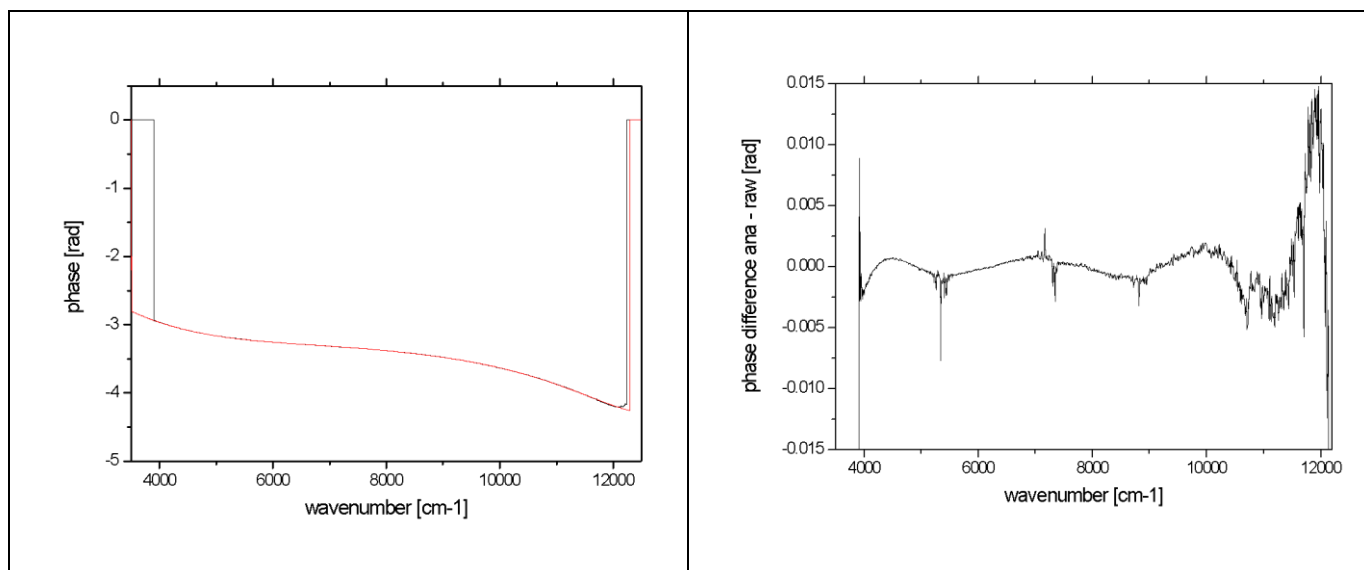
274

275 Figure 2: IRCube phase spectrum. Left panel: raw phase (black) and fitted model (red). Right panel: difference between
276 model (analytical, ana) and raw phase (raw). The gaps in the raw phase are due to opaque spectral sections.

277

278 4.3 Phase spectrum of the IFS125HR FTS operated at Izaña

279 The phase spectrum of the IFS125HR operated at the Izaña observatory is shown in Figure 3. The spectral bandpass covers
280 4000 to beyond 12 000 cm⁻¹. Due to the facts that Izaña is a high-altitude site and a low threshold value for the phase
281 calculation was used because of the very low noise level of the measurements, there are no gaps in the raw phase. Some
282 structure can be seen in the model minus raw phase difference, but this is still within mostly 2 mrad apart from the highest
283 wavenumbers. The curvature of the phase is somewhat stronger than in case of the IRCube. The sharp peaks occurring
284 around 5400 and 7200 cm⁻¹ are coinciding with near-opaque regions of the spectrum and might hint at superimposed
285 spurious signals, potentially due to residual nonlinearity. Such spurious signals generally possess a phase orientation
286 different from the real signal. This finding demonstrates that the model-fitting approach presented here might also be useful
287 for detecting different kinds of imperfections in measured spectra.



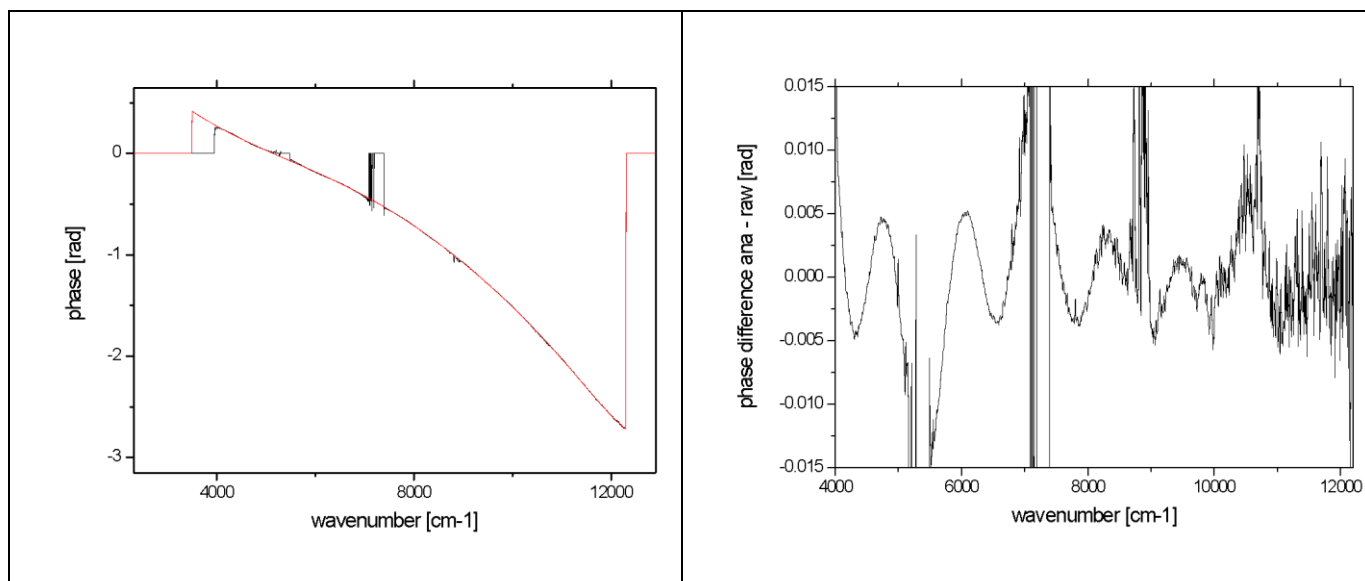
288

289 Figure 3: IFS125HR phase spectrum. Left panel: raw phase (black) and fitted model (red). Right panel: difference between
290 model (analytical, ana) and raw phase (raw).

291 4.4 Phase spectrum of the Vertex 70 FTS

292 Figure 4 shows the phase spectrum of the Vertex 70 FTS. The spectral range covered extends from around 4000 to beyond
293 12 000 cm^{-1} . It is the most unusual phase spectrum we found, showing pronounced quasi-periodic oscillations of about 600
294 cm^{-1} cycle length in the raw phase (see right panel), which cannot be fitted by the polynomial model used. The amplitude of
295 these oscillations amounts to ± 5 mrad. A very similar oscillatory structure is present in the successor of this spectrometer
296 offered by Bruker under the model name Invenio (not shown here). We reported back our findings to the manufacturer, but
297 so far no explanation or remedy for the unusual behaviour was found. Again, it turns out that the approach presented here to
298 fit a smooth model phase to the raw phase is useful for discovering such instrumental characteristics which otherwise remain
299 overlooked. If the approach presented here is to be applied in an operational way for Invenio measurements, a specific model
300 extension must be designed that allows to reproduce the oscillatory features found in the raw phase.

301



302

303 Figure 4: Vertex 70 phase spectrum. Left panel: raw phase (black) and fitted model (red). Right panel: difference between
304 model and raw phase. The gaps in the raw phase are due to opaque spectral sections.

305

306

307 5 Impact of the phase on the spectrum and on retrieved gas columns

308 Figure 5 shows the effect of using either the Mertz or the analytical phase when calculating the spectrum from the measured
309 interferogram. We here use the EM27/SUN and the IRcube for illustration and we investigate the spectral region used for the
310 analysis of CO₂ (~ 6200 – 6400 cm⁻¹). The EM27/SUN phase spectrum is nearest to a straight line, and the differences
311 between Mertz and analytical phase are well within 1 mrad in the CO₂ region (see Figure 1). The IRcube phase spectrum has
312 stronger curvature, but the model used for the analytical phase still delivers a good fit. The differences between Mertz and
313 analytical phase are mostly within 2 mrad in the CO₂ region (see Figure 2).

314

315 According to Figure 5, the spectral differences of the IRcube spectra are significantly larger than for the EM27/SUN. This
316 reminds of the fact that double-sided interferogram recording has an important intrinsic advantage over single-sided
317 interferograms, because the propagation of a phase error into the spectrum is much more critical for single-sided
318 interferograms. While sine contributions emerging from $\pm OPD$ cancel out in double-sided interferograms, they give rise to
319 point-symmetric residuals around spectral lines in spectra generated from single-sided interferograms. Securing an optimized



320 phase reconstruction is of higher importance for single-sided interferograms (all the spectrometers investigated here apart
321 from the EM27/SUN) than for the EM27/SUN, which essentially is insensitive to phase errors in reasonable limits.

322

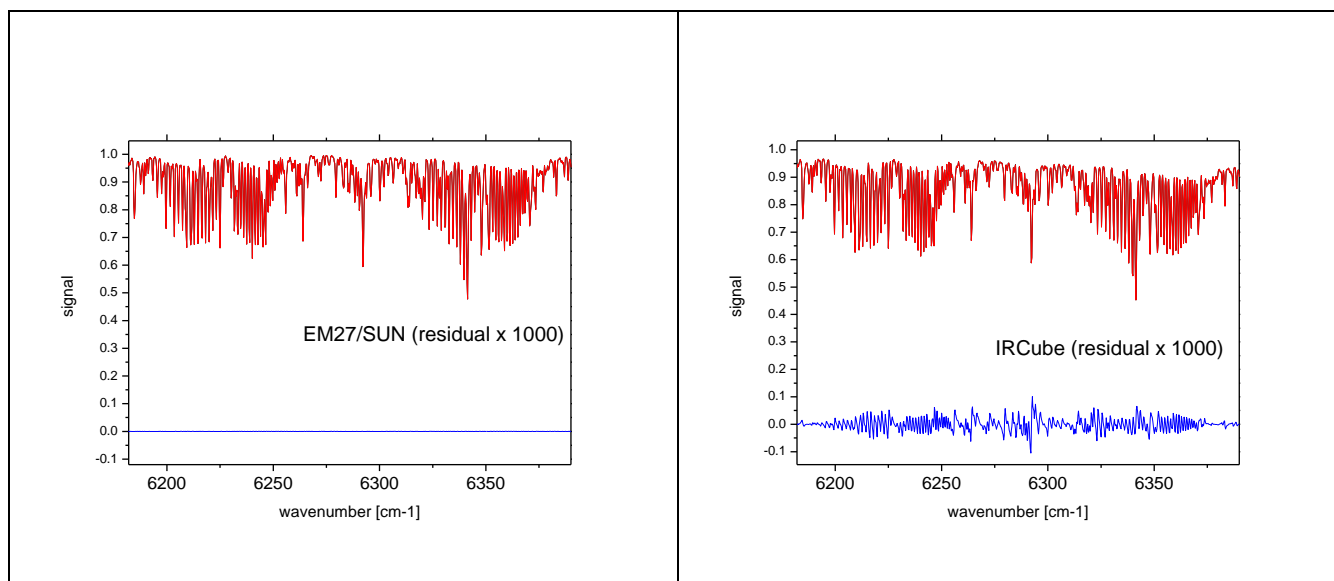
323 The spectral residuals found for the IRcube are quite moderate (below the 10^{-4} level), on the other hand both the increasing
324 demands to be met for the validation of new space borne GHG missions as well as the desired ability to quantify local
325 sources from differential column measurements make XCO₂ measurements with accuracies in the 0.05 ppm range desirable
326 ($\sim 10^{-4}$).

327

328 The analysis of the IRcube spectra indicates a change of CO₂ column of about $2 \cdot 10^{-5}$ between the two phase corrections
329 methods, which is not expected to dominate the IRcube error budget. But other tested spectrometer types showed more
330 pronounced spectral structures in the phase (factor two to five higher amplitudes), which are not negligible.

331

332 In general, there is no guarantee that the analytical phase solution is nearer to the truth than the Mertz phase spectrum. The
333 results always need to be evaluated in context of the specific application. The analytical model might require extensions to
334 include unexpected phase oscillations (as for the Vertex 70). In any case, however, the analytical method is highly useful to
335 carve out unexpected structures in the Mertz phase, which are easily overlooked without performing a comparison to the
336 smooth analytical phase. A careful analysis of such features might help to further improve the design of interferometers and
337 supports recognition of instrumental problems, because the non-local spectral artefacts created by various error sources (as
338 nonlinearity, sampling ghosts, double passing) also create disturbances of the phase spectrum.



339



340 Figure 5: differences of spectra as resulting from the Mertz phase correction scheme and the analytical phase approach. Left:
341 EM27/SUN, right: IRCube, the spectral residuals are enlarged by a factor of 1000.

342

343 **6 Summary and Conclusion**

344 We have implemented a refined method for reconstructing the phase spectrum of FTIR spectrometers. We have applied the
345 new method to different types of spectrometers and found pronounced differences in phase imperfections between them. Our
346 findings demonstrate the usefulness of the method proposed both for operational work and instrumental diagnosis. The
347 proposed algorithm has been incorporated in the COCCON pre-processing code, which is available under the GNU General
348 Public License version 3.

349

350

351

352 **Authors Share**

353 FH has implemented the new method for phase correction using analytical model fits of the phase spectrum. He has
354 generated the results for the different spectrometers investigated in this work and wrote the predominant part of the
355 manuscript. All authors have studied and commented on the manuscript.

356

357 **Competing Interests**

358 At least one of the (co-)authors is a member of the editorial board of Atmospheric Measurement Techniques.

359

360 **Acknowledgements**

361 The establishment of the Izaña TCCON site was supported by grants from NASA's terrestrial carbon cycle program and
362 from the OCO project office.

363

364 **Financial Support**

365 This research has been supported by the European Space Agency (contract 400136108/21/I-DT-lr).

366

367 **Code Availability**

368 The COCCON software suite including the pre-processing software PREPROCESS is made available under GPL version 3
369 license. From version 2.3 onwards, it supports the option of using the analytical phase model implemented in



370 PREPROCESS. The software suite and source codes are available for download at <https://www.imk->
371 [asf.kit.edu/english/3225.php](https://www.imk-asf.kit.edu/english/3225.php).

372

373 **References**

374

375 Alberti, C., Hase, F., Frey, M., Dubravica, D., Blumenstock, T., Dehn, A., Castracane, P., Surawicz, G., Harig, R., Baier, B.
376 C., Bès, C., Bi, J., Boesch, H., Butz, A., Cai, Z., Chen, J., Crowell, S. M., Deutscher, N. M., Ene, D., Franklin, J. E., García,
377 O., Griffith, D., Grouiez, B., Grutter, M., Hamdouni, A., Houweling, S., Humpage, N., Jacobs, N., Jeong, S., Joly, L., Jones,
378 N. B., Jouglet, D., Kivi, R., Kleinschek, R., Lopez, M., Medeiros, D. J., Morino, I., Mostafavipak, N., Müller, A., Ohyama,
379 H., Palmer, P. I., Pathakoti, M., Pollard, D. F., Raffalski, U., Ramonet, M., Ramsay, R., Sha, M. K., Shiomi, K., Simpson,
380 W., Stremme, W., Sun, Y., Tanimoto, H., Té, Y., Tsidu, G. M., Velazco, V. A., Vogel, F., Watanabe, M., Wei, C., Wunch,
381 D., Yamasoe, M., Zhang, L., and Orphal, J.: Improved calibration procedures for the EM27/SUN spectrometers of the
382 COLlaborative Carbon Column Observing Network (COCCON), *Atmos. Meas. Tech.*, 15, 2433–2463,
383 <https://doi.org/10.5194/amt-15-2433-2022>, 2022.

384

385 P. F. Bernath, C. T. McElroy, M. C. Abrams, C. D. Boone, M. Butler, C. Camy-Peyret, M. Carleer, C. Clerbaux, P.-F.
386 Coheur, R. Colin, P. DeCola, M. DeMazière, J. R. Drummond, D. Dufour, W. F. J. Evans, H. Fast, D. Fussen, K.
387 Gilbert, D. E. Jennings, E. J. Llewellyn, R. P. Lowe, E. Mahieu, J. C. McConnell, M. McHugh, S. D. McLeod, R.
388 Michaud, C. Midwinter, R. Nassar, F. Nichitiu, C. Nowlan, C. P. Rinsland, Y. J. Rochon, N. Rowlands, K. Semeniuk,
389 P. Simon, R. Skelton, J. J. Sloan, M.-A. Soucy, K. Strong, P. Tremblay, D. Turnbull, K. A. Walker, I. Walkty, D. A.
390 Wardle, V. Wehrle, R. Zander, and J. Zou: Atmospheric Chemistry Experiment (ACE): Mission overview, *Geophys. Res.*
391 *Lett.*, 32, L15S01, doi:10.1029/2005GL022386, 2005.

392

393 Brasunas, J. C. and Cushman, G. M.: Uniform Time sampling Fourier Transform Spectroscopy, *Appl. Optics*, 36, 2206–
394 2210, doi:10.1364/AO.36.002206, 1997.

395

396 Brault, J. W.: New approach to high-precision Fourier transform spectrometer design, *Appl. Optics*, 35, 2891–2896,
397 doi:10.1364/AO.35.002891, 1996.

398

399 Davis, S. P., Abrams, M. C. & Brault, J. W. *Fourier Transform Spectrometry*, Academic Press, San Diego, 2001.

400



- 401 De Mazière, M., Thompson, A. M., Kurylo, M. J., Wild, J. D., Bernhard, G., Blumenstock, T., Braathen, G. O., Hannigan, J.
402 W., Lambert, J.-C., Leblanc, T., McGee, T. J., Nedoluha, G., Petropavlovskikh, I., Seckmeyer, G., Simon, P. C., Steinbrecht,
403 W., and Strahan, S. E.: The Network for the Detection of Atmospheric Composition Change (NDACC): history, status and
404 perspectives, *Atmos. Chem. Phys.*, 18, 4935–4964, <https://doi.org/10.5194/acp-18-4935-2018>, 2018.
- 405
- 406 Fischer, H., Birk, M., Blom, C., Carli, B., Carlotti, M., von Clarmann, T., Delbouille, L., Dudhia, A., Ehhalt, D., Endemann,
407 M., Flaud, J. M., Gessner, R., Kleinert, A., Koopman, R., Langen, J., López-Puertas, M., Mosner, P., Nett, H., Oelhaf, H.,
408 Perron, G., Remedios, J., Ridolfi, M., Stiller, G., and Zander, R.: MIPAS: an instrument for atmospheric and climate
409 research, *Atmos. Chem. Phys.*, 8, 2151–2188, <https://doi.org/10.5194/acp-8-2151-2008>, 2008.
- 410
- 411 Forman, M. L., Steel, W. H. & Vanasse, G. A. Correction of asymmetric interferograms obtained in Fourier spectroscopy. *J.*
412 *Opt. Soc. Am.* 56, 59–63, 1966.
- 413
- 414 Frey, M., Sha, M. K., Hase, F., Kiel, M., Blumenstock, T., Harig, R., Surawicz, G., Deutscher, N. M., Shiomi, K., Franklin,
415 J. E., Bösch, H., Chen, J., Grutter, M., Ohshima, H., Sun, Y., Butz, A., Mengistu Tsidu, G., Ene, D., Wunch, D., Cao, Z.,
416 Garcia, O., Ramonet, M., Vogel, F., and Orphal, J.: Building the COllaborative Carbon Column Observing Network
417 (COCCON): long-term stability and ensemble performance of the EM27/SUN Fourier transform spectrometer, *Atmos.*
418 *Meas. Tech.*, 12, 1513-1530, <https://doi.org/10.5194/amt-12-1513-2019>, 2019.
- 419
- 420 Friedl-Vallon, F., Gulde, T., Hase, F., Kleinert, A., Kulesa, T., Maucher, G., Neubert, T., Olschewski, F., Piesch, C.,
421 Preusse, P., Rongen, H., Sartorius, C., Schneider, H., Schönfeld, A., Tan, V., Bayer, N., Blank, J., Dapp, R., Ebersoldt, A.,
422 Fischer, H., Graf, F., Guggenmoser, T., Höpfner, M., Kaufmann, M., Kretschmer, E., Latzko, T., Nordmeyer, H., Oelhaf, H.,
423 Orphal, J., Riese, M., Schardt, G., Schillings, J., Sha, M. K., Suminska-Ebersoldt, O., and Ungermann, J.: Instrument concept
424 of the imaging Fourier transform spectrometer GLORIA, *Atmos. Meas. Tech.*, 7, 3565–3577, <https://doi.org/10.5194/amt-7-3565-2014>, 2014.
- 425
- 426
- 427 García, O. E., Schneider, M., Sepúlveda, E., Hase, F., Blumenstock, T., Cuevas, E., Ramos, R., Gross, J., Barthlott, S.,
428 Röhling, A. N., Sanromá, E., González, Y., Gómez-Peláez, Á. J., Navarro-Comas, M., Puentedura, O., Yela, M., Redondas,
429 A., Carreño, V., León-Luis, S. F., Reyes, E., García, R. D., Rivas, P. P., Romero-Campos, P. M., Torres, C., Prats, N.,
430 Hernández, M., and López, C.: Twenty years of ground-based NDACC FTIR spectrometry at Izaña Observatory – overview
431 and long-term comparison to other techniques, *Atmos. Chem. Phys.*, 21, 15519–15554, <https://doi.org/10.5194/acp-21-15519-2021>, 2021.
- 432
- 433



- 434 Gisi, M., Hase, F., Dohe, S., and Blumenstock, T.: Camtracker: a new camera controlled high precision solar tracker system
435 for FTIR-spectrometers, *Atmos. Meas. Tech.*, 4, 47–54, <https://doi.org/10.5194/amt-4-47-2011>, 2011.
- 436
- 437 Gisi, M., Hase, F., Dohe, S., Blumenstock, T., Simon, A., and Keens, A.: XCO₂-measurements with a Tabletop FTS Using
438 Solar Absorption Spectroscopy, *Atmospheric Measurement Techniques*, 5, 2969–2980, [https://doi.org/10.5194/amt-5-2969-](https://doi.org/10.5194/amt-5-2969-2012)
439 2012, 2012.
- 440
- 441 Griffiths, P. R., and De Haseth, J. A.: *Fourier Transform Infrared Spectrometry*, John Wiley & Sons Inc., Hoboken, 2007.
- 442
- 443 Hase, F., M. Frey, M. Kiel, T. Blumenstock, R. Harig, A. Keens, and J. Orphal: Addition of a channel for XCO observations
444 to a portable FTIR spectrometer for greenhouse gas measurements, *Atmos. Meas. Tech.*, 9, 2303-2313, doi:10.5194/amt-9-
445 2303-2016, 2016.
- 446
- 447 Hase, F., M. Frey, T. Blumenstock, J. Groß, M. Kiel, R. Kohlhepp, G. Mengistu Tsidu, K. Schäfer, M. K. Sha, and J. Orphal:
448 Application of portable FTIR spectrometers for detecting greenhouse gas emissions of the major city Berlin, *Atmos. Meas.*
449 *Tech.*, 8, 3059-3068, doi:10.5194/amt-8-3059-2015, 2015.
- 450
- 451 Herres, W. & Gronholz, J. Understanding FT-IR data processing. Part 2: Details of the spectrum calculation. *Intell. Instrum.*
452 *Comput., Appl. Lab.* 3, 10–19, 1985.
- 453
- 454 Kille, N., Chiu, R., Frey, M., Hase, F., Sha, M. K., Blumenstock, T., Hannigan, J.W., Orphal, J.W., Bon, D. and Volkamer,
455 R.: Separation of methane emissions from agricultural and naturalgas sources in the Colorado Front Range, *Geophysical*
456 *Research Letters*, 46, <https://doi.org/10.1029/2019GL08213>, 2019.
- 457
- 458 Richard C. M. Learner, Anne P. Thorne, Ian Wynne-Jones, James W. Brault, and Mark C. Abrams: Phase correction of
459 emission line Fourier transform spectra, *J. Opt. Soc. Am. A* 12, 2165-2171, 1995.
- 460
- 461 Luther, A., Kleinschek, R., Scheidweiler, L., Defratyka, S., Stanisavljevic, M., Forstmaier, A., Dandocsi, A., Wolff, S.,
462 Dubravica, D., Wildmann, N., Kostinek, J., Jöckel, P., Nickl, A.-L., Klausner, T., Hase, F., Frey, M., Chen, J., Dietrich, F.,
463 Nęcki, J., Swolkień, J., Fix, A., Roiger, A., and Butz, A.: Quantifying CH₄ emissions from hard coal mines using mobile
464 sun-viewing Fourier transform spectrometry, *Atmos. Meas. Tech.*, 12, 5217–5230, [https://doi.org/10.5194/amt-12-5217-](https://doi.org/10.5194/amt-12-5217-2019)
465 2019, 2019.
- 466



- 467 Luther, A., Kostinek, J., Kleinschek, R., Defratyka, S., Stanisavljević, M., Forstmaier, A., Dandocsi, A., Scheidweiler, L.,
468 Dubravica, D., Wildmann, N., Hase, F., Frey, M. M., Chen, J., Dietrich, F., Nęcki, J., Swolkień, J., Knote, C., Vardag, S. N.,
469 Roiger, A., and Butz, A.: Observational constraints on methane emissions from Polish coal mines using a ground-based
470 remote sensing network, *Atmos. Chem. Phys.*, 22, 5859–5876, <https://doi.org/10.5194/acp-22-5859-2022>, 2022.
- 471
- 472 Mertz, L., *Transformations in Optics*, John Wiley and Sons, Inc., New York, 1965.
- 473
- 474 Schneider, M., Blumenstock, T., Chipperfield, M. P., Hase, F., Kouker, W., Reddman, T., Ruhnke, R., Cuevas, E., and
475 Fischer, H.: Subtropical trace gas profiles determined by groundbased FTIR spectroscopy at Izaña (28° N, 16° W): Five-year
476 record, error analysis, and comparison with 3-D CTMs, *Atmos. Chem. Phys.*, 5, 153–167, [https://doi.org/10.5194/acp-5-](https://doi.org/10.5194/acp-5-153-2005)
477 153-2005, 2005.
- 478
- 479 Schneider, M., Sepúlveda, E., García, O., Hase, F., and Blumenstock, T.: Remote sensing of water vapour profiles in the
480 framework of the Total Carbon Column Observing Network (TCCON), *Atmos. Meas. Tech.*, 3, 1785–1795,
481 <https://doi.org/10.5194/amt-3-1785-2010>, 2010.
- 482
- 483 Sha, M. K., De Mazière, M., Notholt, J., Blumenstock, T., Chen, H., Dehn, A., Griffith, D. W. T., Hase, F., Heikkinen, P.,
484 Hermans, C., Hoffmann, A., Huebner, M., Jones, N., Kivi, R., Langerock, B., Petri, C., Scolas, F., Tu, Q., and Weidmann,
485 D.: Intercomparison of low- and high-resolution infrared spectrometers for ground-based solar remote sensing measurements
486 of total column concentrations of CO₂, CH₄, and CO, *Atmos. Meas. Tech.*, 13, 4791–4839, [https://doi.org/10.5194/amt-13-](https://doi.org/10.5194/amt-13-4791-2020)
487 4791-2020, 2020.
- 488
- 489 M.K. Sha et al., *Remote Sensing 2024* (Manuscript ID: remotesensing-3148670) submitted on 25 July 2024.
- 490
- 491 Tu, Q., Hase, F., Schneider, M., García, O., Blumenstock, T., Borsdorff, T., Frey, M., Khosrawi, F., Lorente, A., Alberti, C.,
492 Bustos, J. J., Butz, A., Carreño, V., Cuevas, E., Curcoll, R., Diekmann, C. J., Dubravica, D., Ertl, B., Estruch, C., León-Luis,
493 S. F., Marrero, C., Morgui, J.-A., Ramos, R., Scharun, C., Schneider, C., Sepúlveda, E., Toledano, C., and Torres, C.:
494 Quantification of CH₄ emissions from waste disposal sites near the city of Madrid using ground- and space-based
495 observations of COCCON, TROPOMI and IASI, *Atmos. Chem. Phys.*, 22, 295–317, [https://doi.org/10.5194/acp-22-295-](https://doi.org/10.5194/acp-22-295-2022)
496 2022, 2022.
- 497
- 498 D. Wunch, G.C. Toon, J.-F.L. Blavier, R.A. Washenfelder, J. Notholt, B.J. Connor, D.W.T. Griffith, V. Sherlock, P.O.
499 Wennberg. The Total Carbon Column Observing Network. *Phil. Trans. R. Soc. A*, 369, doi:10.1098/rsta.2010.0240, 2011.
- 500



501 Yokota, T., Yoshida, Y., Eguchi, N., Ota, Y., Tanaka, T., Watanabe, H., and Maksyutov, S.: Global Concentrations of CO₂
502 and CH₄ Retrieved from GOSAT: First Preliminary Results, SOLA, 5, 160–163, <https://doi.org/10.2151/sola.2009-041>,
503 2009.

504

505 M. Zhou, B. Langerock, M. K. Sha, C. Hermans, N. Kumps, R. Kivi, P. Heikkinen, C. Petri, J. Notholt, H. Chen, and M. De
506 Mazière. Atmospheric n₂o and ch₄ total columns retrieved from low-resolution fourier transform infrared (ftir) spectra
507 (bruker vertex 70) in the mid-infrared region. Atmospheric Measurement Techniques, 16 (22): 5593–5608, 2023. doi:
508 10.5194/amt-16-5593-2023.

509